THE JOURNAL OF PHYSICAL CHEMISTRY C
A JOURNAL OF THE AMERICAN CHEMICAL SOCIETY

pubs.acs.org/JPCC

Article

Quasi-Hexagonal to Lepidocrocite-like Transition in TiO_2 Ultrathin Films on Cu(001)

Andrea Luigi Sorrentino, Giulia Serrano,* Lorenzo Poggini, Brunetto Cortigiani, Khaled E. El-Kelany, Maddalena D'Amore, Anna Maria Ferrari, Andrea Atrei, Andrea Caneschi, Roberta Sessoli, and Matteo Mannini*

Cite This: *J. Phys. Chem. C* 2021, 125, 10621−10630

Read Online

ACCESS | Metrics & More | Article Recommendations | Supporting Information

ABSTRACT: The structure and growth mechanism of TiO_2 ultrathin films on Cu(001) were investigated by experimental and theoretical studies. Multiple experimental techniques, including photoemission spectroscopies and scanning probe microscopy, were used to carefully characterize the chemical, electronic, and morphological structure of the metal oxide layer. A complete and flat TiO_2 bilayer with a lepidocrocite-like structure is observed at the earliest stages of its growth on the Cu(001) surface under controlled experimental conditions. The employed multitechnique approach reveals that a transition between two different structures of the TiO_2 film, that is, the quasi-hexagonal and lepidocrocite-like structure, occurs as a function of the coverage passing from one to two monolayers. *Ab initio* calculations indicate that the lepidocrocite-like structure is thermodynamically more stable on Cu(001) than the quasi-hexagonal one, thus supporting the observed transition.

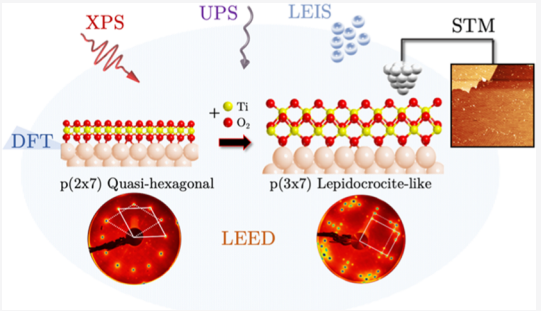

INTRODUCTION

In the last decades, metal oxides have assumed growing importance in multiple technological fields such as catalysis,[1] photovoltaics,[2] and electronics.[3] Thanks to the possibility of developing nanostructured thin films and controlling their electronic properties, metal oxides have also been used for advanced applications, such as tunnel junctions in spintronic devices.[4] Among metal oxides, titanium dioxide (TiO_2), showing a wide band gap and high dielectric constant,[5,6] is one of the most technologically relevant materials, whose use is now widespread in electronics[7] and optoelectronics.[8] Multifunctional electronic devices could also take advantage of the richness of structural phases with different electronic properties of TiO_2 films, which can be achieved by fine-tuning the preparation protocols.[9−14] The most common TiO_2 structures of both bulk phase[15] and nanoparticles[16] are rutile and anatase. On metals, TiO_2 thin films are commonly found as a stable lepidocrocite-like (**LL**) structure but other structures such as the quasi-hexagonal (**QH**) one were also reported.[17−20] The TiO_2 ultrathin film can be used to enhance the power conversion efficiency of the solar cell by reducing the electron−hole recombination on the ZnO surface.[21] Furthermore, theoretical and experimental studies on the TiO_2-**LL** structure were carried out, evidencing its potentialities on multiple fields, such as improved catalytic applications,[22,23] electrode materials,[24] or as an alternative decoupling layer used to preserve the magnetic properties of atoms and molecules deposited on metals.[25−28] Controlling the fabrication of these ultrathin film oxide structures is crucial for their use in technological application, but a deep understanding of the growth processes is also required. Noticeably, the growth of the **LL** structure, which is the most stable TiO_2 film phase on different metal surfaces such as W(100),[9] Ag(100),[17] Pt(111),[10] and Pt(110),[12] critically depends on the deposition conditions.[10,29] In fact, on other metal surfaces such as Cu(001), only TiO_2 films with hexagonal structures were observed.[19,20]

Here, we investigate the early stages of the growth of an ultrathin TiO_2 film on a Cu(001) single crystal and the mechanism that leads to the transition from the **QH** to **LL** phase, when passing from the monolayer to the bilayer thickness of the TiO_2 film. We provide a detailed experimental and theoretical characterization of this system by monitoring the TiO_2 film structural transformation as a function of the surface coverage. The chemical composition of the TiO_2 films was studied by X-ray photoelectron spectroscopy (XPS) and low-energy ion scattering (LEIS) measurements. At the same time, structural properties were characterized by low-energy electron diffraction (LEED) and scanning tunneling micros-

Received: February 6, 2021
Revised: April 13, 2021
Published: May 10, 2021

https://doi.org/10.1021/acs.jpcc.1c01098
J. Phys. Chem. C 2021, 125, 10621−10630

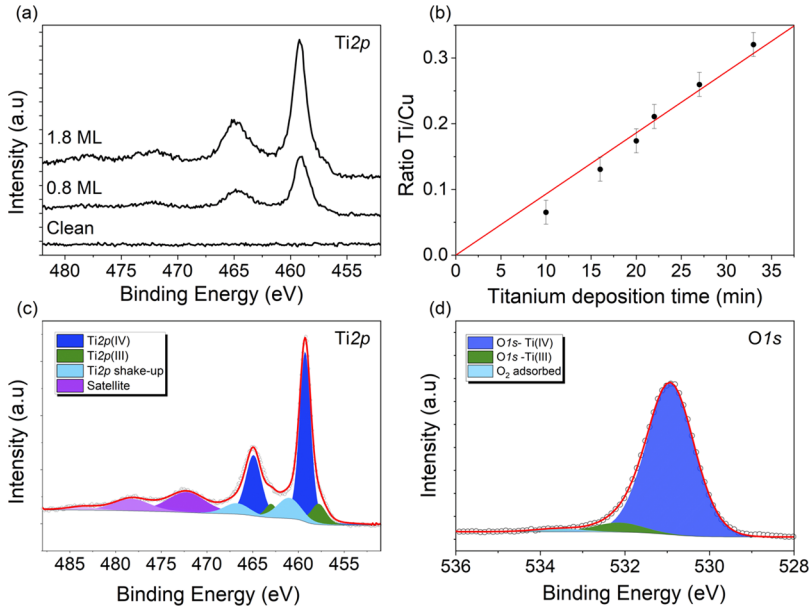

Figure 1. (a) XPS spectra of the clean Cu(001) surface and after the TiO_2 film deposition for 0.8 ML and 1.8 ML. (b) Ti 2p/Cu 2p ratio of the XPS signal area as a function of the titanium deposition time (point corresponds to all the probed coverages between 0.4 and 1.8 ML). XPS spectra of Ti 2p (c) and O 1s (d) regions of TiO_2/Cu at 1.8 ML.

copy (STM). Density functional theory (DFT) calculations were used to rationalize the structure of the supported films and provide a full explanation of the observed structural transition from the **QH** to the **LL** structure as a function of the TiO_2 film thickness. The electronic structure of the surface was then studied by combining the calculated density of states (DOS) and the experimental ultraviolet photoelectron spectroscopy (UPS) results.

EXPERIMENTAL METHODS

Cu(001) crystals were purchased from the Surface Preparation Laboratory (SPL, The Netherlands). The Cu(001) surface was prepared by several cycles of argon ion sputtering (1500 eV) and annealing (770 K) in ultrahigh vacuum (UHV) before the TiO_2 film deposition. Titanium (purity 99.999%) was deposited by employing an electron beam Omicron EFM3 microevaporator. The deposition rate was monitored using the integrated flux monitor of the EFM3 and evaluated *a posteriori* by XPS and STM measurements. The TiO_2 coverage (θ_{TiO_2}) for each deposition step was estimated using the Ti 2p and Cu 2p XPS signals, using the protocol described in the Supporting Information (XPS section). The surface coverage is expressed in the monolayer (ML), see eq S2 reported in the Supporting Information.[30] The TiO_2 film was grown by consecutive doses of titanium until a maximum coverage of about 2 ML was reached. Before the Ti deposition, the Cu(001) substrate, kept at the constant temperature of 570 K, was exposed to an oxygen partial pressure of $pO_2 \approx 1 \times 10^{-6}$ mbar to provide the oxygen amount to grow the first TiO_2 layer. For TiO_2 thickness above 1 ML, the Ti depositions were carried out at $pO_2 \approx 1 \times 10^{-6}$ mbar. After each deposition step, the sample was annealed at *ca.* 770 K. Identical results were obtained by growing the TiO_2 film on different Cu(001) crystals from SPL.

XPS data were acquired using a microfocused monochromatic Al Kα radiation (hν = 1486.6 eV, SPECS mod. XR-MS focus 600) operating at a power of 100 W (13 kV and 7.7 mA) and a multichannel detector electron analyzer, model SPECS Phoibos 150 1DLD (the latter was used for LEIS and UPS measurement). XPS spectra were recorded in normal emission with the X-ray source mounted at an angle of 54.44° to the analyzer. The spectra were collected at normal emission, and the pass energy was set to 40 eV. XPS spectra were calibrated to the Cu $2p_{3/2}$ signal at 932.7 eV, and the background was subtracted using the Shirley method.[31] A 70−30% combination of Gaussian and Lorentzian functions was employed to fit the spectra. LEIS spectra were acquired using a focused He^+ ion beam generated by an Omicron ISE 100 Gun with an energy of 1.0 keV impinging the surface at an angle of 45°. LEED patterns were acquired using an Omicron three-grid optics, model NG-LEED. UPS data were collected using a nonmonochromatized gas discharge UV lamp (VG Scientific 22-101) using the He(II) line (40.8 eV). The analyzer pass energy was set to 10 eV, and a fixed bias of −30 V was applied to the sample. UPS spectra were measured at normal emission and calibrated to the Fermi energy of Cu(001). STM measurements were carried out under UHV conditions at room temperature using a variable temperature (VT)-STM Omicron (model XA VT-STM) with electrochemically etched W tips.

COMPUTATIONAL DETAILS

In this section, the main information concerning methods and models adopted in the DFT calculations are reported. Additional details can be found in the DFT section of the Supporting Information.

DFT calculations were performed with a periodic approach, using a localized Gaussian-type function basis set implemented in the CRYSTAL17 code.[32] The pure GGA (generalized gradient-corrected) Perdew−Wang (PW91) exchange−correlation functional was used to reproduce the properties of both the metal and oxide satisfactorily.[17,20] To account for noncovalent interactions at the interface, the semiempirical D2* correction (based on Grimme's correction[33] refitted for crystalline systems) has been combined with the hybrid PBE0 and B3LYP functionals, since these combined schemes have

https://doi.org/10.1021/acs.jpcc.1c01098
J. Phys. Chem. C 2021, 125, 10621−10630

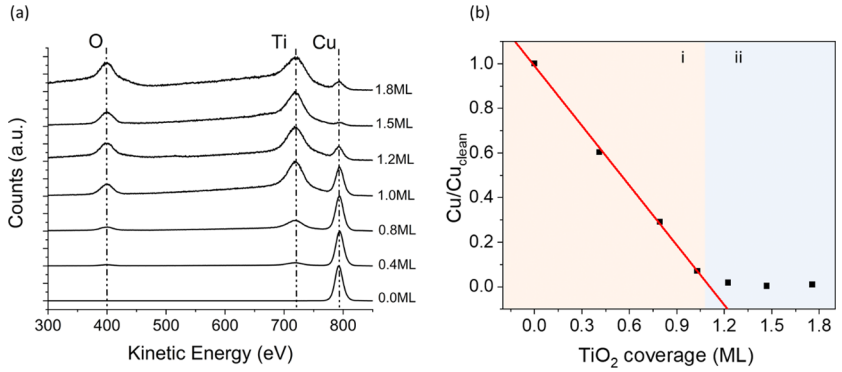

Figure 2. (a) LEIS spectra of TiO_2/Cu at different coverages; (b) intensity of the normalized LEIS Cu signal as a function of the TiO_2 film coverage below (region i) and above (region ii) 1 ML.

been found to successfully describe surface interactions.[34,35] Basis sets of triple-ζ quality for the valence electrons have been adopted for all atoms.

For surface calculations, CRYSTAL17 adopts periodic slab models characterized by two infinite dimensions (x and y) and a finite thickness along the z-direction. The geometry of the metal slab dictates the 2D unit cell of the overlayer considered. The $p(3 \times 7)$ and $p(2 \times 7)$ coincidence cells (Cu supercells) were used for supported **LL** and **QH** structures of TiO_2, respectively, as derived by LEED analysis.

To characterize the interaction between the metal and the oxide and the relative stability of the TiO_2 overlayers, we computed the adhesion energy E_{adh} (per surface unit) according to the following equation

$$E_{adh} = \frac{E_{TiO_2/Cu} - E_{TiO_2} - E_{Cu}}{2S} \quad (1)$$

where $E_{TiO_2/Cu}$ is the total energy of the heterostructure, E_{Cu} is the total energy of the metal substrate, and E_{TiO_2} is the total energy of the oxide overlayer relaxed at the same lattice parameters of the substrate. The factor 2 in the denominator accounts for the two outer surfaces since double-sided adsorption has been considered.

The total interface energy has been computed according to the following relation

$$E_{adh}^{str} = E_{adh} + E^{str} \quad (2)$$

it is, indeed, the sum of the adhesion energy and the strain energy, E^{str}, the energy difference between the fully relaxed oxide films and the films relaxed at the substrate coincidence cell. All reported adhesion energies have been corrected for the basis set superposition error, BSSE.

UPS spectra were simulated by computing the density of states projected on O 2p, Ti 3d, and Cu 3d together with Cu 4s orbitals for both the **QH** $p(2 \times 7)$ and the **LL** $p(3 \times 7)$ phases. For each subshell, the contribution was then weighted by its cross section at the He(II) energy (40.8 eV).

RESULTS AND DISCUSSIONS

Chemical Investigation by XPS and LEIS. XPS was used to evaluate the chemical composition during the growth of the TiO_2 film on the Cu(001) surface (TiO_2/Cu, hereafter). Figure 1a reports the Ti 2p XPS region for the clean Cu(001) surface (bottom) and two different surface coverages (0.8 ML and 1.8 ML), showing the progressive increase in the Ti 2p signal. Figure 1b shows that the ratio between the areas of Ti 2p and Cu 2p signals increases linearly with the deposition time, suggesting that TiO_2 islands maintain a similar and uniform thickness during the film growth process, thus excluding a Volmer–Weber growth.[36] The fit of the Ti 2p XPS spectrum reported in Figure 1c shows the main contribution (blue) at 459.2 eV attributable to Ti^{IV} species.[37] Their relative spin–orbit coupling component (Ti $2p_{1/2}$) is shifted by 5.7 eV in line with previous reports.[38] An additional component at lower binding energy (457.9 eV, green) indicates the presence of a small amount of Ti^{III}.[39,40] Its presence is probably the consequence of the annealing process performed after each deposition step to favor the reorganization of the TiO_2 layer. Shake-up components (light blue) are present at higher binding energies (460.8 and 466.5 eV), and additional satellite features from 472.2 to 483.3 eV (dark violet) are observed.[41,42] The O 1s region shows three components (Figure 1d): the main peak located at 530.8 eV (blue) corresponds to oxygen atoms bound to Ti^{IV} atoms in the TiO_2 structure, the peak at 532.1 eV (green) is attributed to oxygen bound to Ti^{III} species (present as Ti_2O_3[40] or is assigned to the oxygen of Ti–OH bonds[43]), and the one evidenced at 533.6 eV (light blue) is due to small traces of H_2O (or OH groups) on the surface of the TiO_2 film.[44,45] The Ti/O XPS signal ratio is about 0.5 for all the investigated coverages (see Figure S1), confirming that the expected film stoichiometry is retained during deposition.[19]

The high surface sensitivity of LEIS was used to further characterize the chemical composition of the termination layer during the TiO_2 film growth. In Figure 2a, LEIS spectra are reported as a function of the surface coverage. The clean Cu(001) spectrum shows a main peak at 793 eV, corresponding to He^+ ions scattered by Cu atoms (see eq S3 in the Supporting Information).[46] At 0.4 ML, two peaks attributable to the scattering by O and Ti atoms appear at 400 and 720 eV, respectively. By increasing the coverage, the Cu peak decreases until it almost disappears at 1.2 ± 0.1 ML. Additional information about the growth mechanism of the oxide film can be obtained by plotting the area of the Cu peak in the LEIS spectra (normalized to that measured on the clean Cu(001) surface) as a function of the film coverage[19] (see Figure 2b). The graph in Figure 2b evidences a linear trend between 0.1 ML and 1.0 ML (region i). This analysis clearly suggests that TiO_2 initially grows as 2D islands.[47] Above 1 ML (region ii), the Cu signal levels to zero within LEIS sensitivity.

LEED-Based Structural Characterization. The crystallographic structure of the TiO_2 film was investigated by LEED between 0 and 1.8 ML (Figure 3). The LEED pattern of the

https://doi.org/10.1021/acs.jpcc.1c01098
J. Phys. Chem. C 2021, 125, 10621–10630

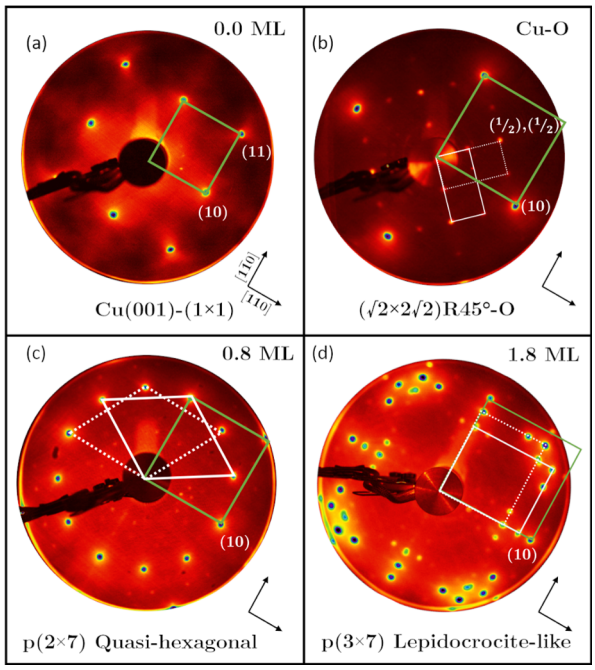

Figure 3. LEED pattern showing surface reconstruction of the TiO_2 film on Cu(001) as a function of the coverage. (a) Cu(001)—(1 × 1) reconstruction (green), 80 eV. (b) Cu−O phase, ($\sqrt{2} \times 2\sqrt{2}$) *R*45°-O reconstruction (white domains) due to the chemisorbed oxygen on copper (see the text). (c) TiO_2-**QH** phase (white domains), 67 eV. (d) TiO_2-**LL** structure (white domains), 57 eV.

clean Cu(001) surface (Figure 3a) shows the (1 × 1) unit cell of the clean Cu(001) surface. As a guide to the eye, a green square marks the clean Cu(001)—(1 × 1) reconstruction in all LEED patterns. The exposure of the clean Cu(001) surface to oxygen performed before the TiO_2 deposition (see details in the Experimental Methods) induces an oxygen chemisorption phase (Cu−O, hereafter) with a ($\sqrt{2} \times 2\sqrt{2}$) *R*45°-O surface reconstruction.[19,48] The LEED pattern of the Cu−O phase (Figure 3b) shows two ($\sqrt{2} \times 2\sqrt{2}$) *R*45°-O domains rotated by 90° (white rectangles in Figure 3b), in line with previous findings.[49−51] After the first Ti deposition (0.4 ML, Figure S2a), additional faint spots superimposed to the ($\sqrt{2} \times 2\sqrt{2}$) *R*45°-O pattern appear and become predominant once they reached 0.8 ML. The LEED pattern at 0.8 ML (Figure 3c) is typical of a **QH** phase of the TiO_2 film and shows two **QH** domains rotated by 30° (features marked as white rhombi).[19,20] This pattern can be described in terms of a *p*(2 × 7) coincidence cell, as already observed for TiO_2 films on Cu(001) at similar low coverage.[19,20] At 1.5 ML, additional spots, marking a rectangular unit cell, appear in the LEED pattern (Figure S2b) and are attributable to an **LL** structure,[17] indicating the occurrence of a transition unprecedently observed on Cu(001). At 1.8 ML (Figure 3c), LEED spots related to the rectangular **LL** structure dominate and show two **LL** domains rotated by 90° (white rectangles) and aligned with the directions of the Cu(001)−(1 × 1) directions. The **LL** unit cell parameters, derived from the LEED pattern, are $a = 0.38 \pm 0.01$ nm and $b = 0.29 \pm 0.01$ nm, thus resulting in close agreement with those reported in the literature for TiO_2 films with an **LL** structure on different metal surfaces.[9,12,17] It is important to note that b is almost coincident with the lattice parameter value of the **QH** structure[20] ($a_{hex} = 0.295$ nm), suggesting that essentially no strain is present along the [110] direction.

The LEED pattern in Figure 3d shows that the TiO_2-**LL** film on Cu(001) has a $p(3 \times 7)$ coincidence cell (see details and transformation matrices in the Supporting Information).

Morphological Characterization by STM. STM images were recorded to evaluate the morphology of the TiO_2 film during the growth process. The clean Cu(001) surface (Figure 4a) is characterized by regular monoatomic steps[52] with a

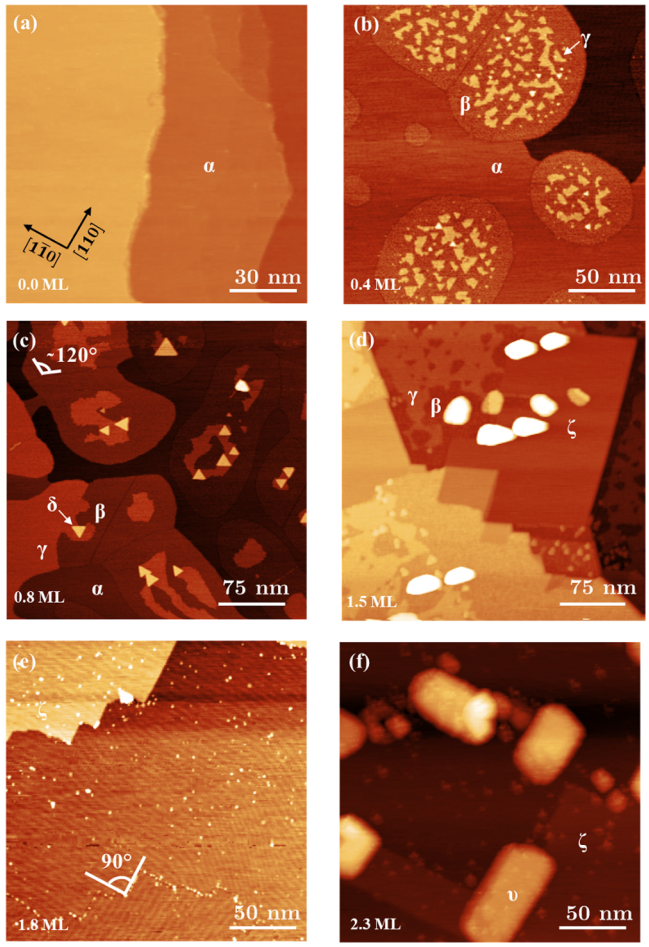

Figure 4. STM images of the TiO_2 film growth on Cu(001) as a function of the coverage. (a) 0.0 ML Cu(001) clean surface (α); (b) 0.4 ML: first (β)- and second (γ)-layer TiO_2 island formation (V = 2.5 V and I_t = 200 pA); (c) 0.8 ML: formation of third-layer TiO_2 islands (δ) with triangular shape (V = 2.0 V and I_t = 200 pA); (d) 1.5 ML: formation of squared patches (ζ) in the TiO_2 film (V = 2.5 V and I_t = 100 pA); (e) 1.8 ML: TiO_2-**LL** structure fully covers the surface. (V = 2.0 V and I_t = 150 pA); (f) 2.3 ML: formation of 3D rectangular islands (υ) on the TiO_2-**LL** layer (V = 2.0 V and I_t = 300 pA).

height of 0.20 ± 0.02 nm (see line profiles in Figure S3). At 0.4 ML (Figure 4b), TiO_2 islands (β) cover about 35% of the clean Cu(001) surface (α), in line with the XPS coverage calibration (Figure 2b). TiO_2 layer islands (β) exhibit an irregular round shape,[19] and their apparent height depends significantly on the applied bias, coherently with literature reports.[53,54] Already at this low coverage, the surface is characterized by the presence of second-layer islands with an almost triangular shape and partially coalescing (γ in Figure 4b). Their height with respect to β islands is 0.25 ± 0.02 nm (see the line profile in Figure S4). At 0.8 ML (Figure 4c), it is

https://doi.org/10.1021/acs.jpcc.1c01098
J. Phys. Chem. C 2021, 125, 10621−10630

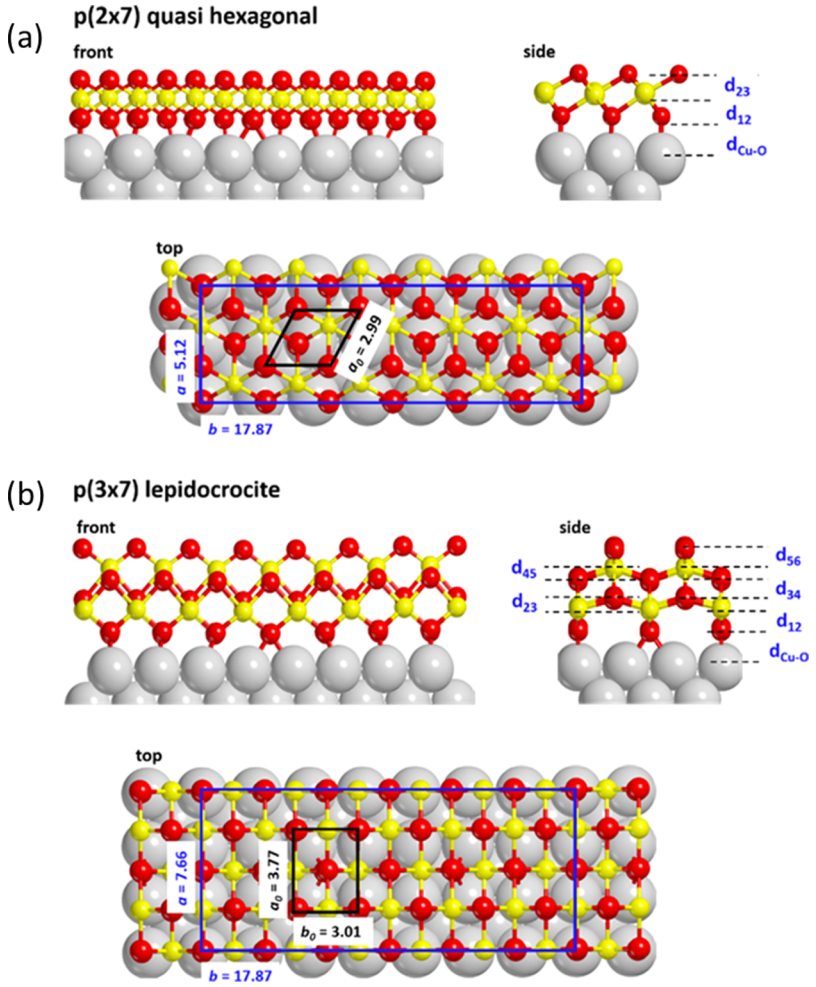

Figure 5. Calculated DFT structure representation of the coincidence cells: (a) **QH**$p(2 \times 7)$ and (b) **LL** $p(3 \times 7)$ of TiO_2 on the Cu(001) surface. For each coincidence, front, side, and top views are reported. In blue, the coincidence cells of the metal; in black, the cell of the unsupported oxide film. Values are reported in Å.

possible to observe the presence of large β islands characterized by domain boundaries that form angles of about 120° (Figure 4c). This angle could be consistent with the hexagonal structure observed in the LEED pattern (Figure 3c) and predicted by literature DFT calculations.[20] The second layer islands (γ) and triangular islands in the third layer (δ) show a height of 0.25 ± 0.02 and 0.45 ± 0.02 nm, respectively (see the line profile in Figure S5). δ islands have a well-defined triangular shape and are rotated by 30° between each other. Their structure could be in agreement with the **QH** domain orientation observed in the LEED pattern of Figure 3c but is observed only at this coverage. Similar triangular-shaped islands have been observed for the TiO_2 film on Au(111)[55] and ZnO on metals.[56] In the last case, the formation of such triangular structures was ascribed to a stabilization effect compensating the polar zinc oxide film.[56] At 1.5 ML, that is, after the full surface coverage has been reached, a change in the film morphology is clearly visible (Figure 4d). Close to irregular TiO_2 islands (β and γ), large and squared patches (ζ) appear on the surface, along with the formation of the TiO_2-**LL** structure in the LEED pattern (Figure S2b). A slight distortion of the angle formed by the boundary of the ζ island (Figure 4d) from the rectangular **LL** structure could be due to kinked step edge structures (a closer look to ζ step edges is reported in Figure S6).[57] At 1.8 ML (Figure 4e), the surface is uniformly covered by a TiO_2-**LL** film. The morphology of the TiO_2 film now shows defined boundary angles of ∼90° and a regular film corrugation, typical of the TiO_2-**LL** films.[17] Similar to the TiO_2 film on Ag(100),[17,58] the corrugation of the **LL** structure evidenced by bright and dark stripes in the STM images of Figure 4e is probably due to the lattice mismatch between the TiO_2 film with the Cu(001) surface. Line profiles in Figure S7 show that the corrugation along the z axis (perpendicularly to the surface) is about 0.3 nm and the lateral periodicity is about 4.5 nm. We also notice that the **LL** film is formed by two perpendicularly oriented domains (Figure S7), in agreement with the LEED patterns (Figure 3d). At the highest investigated coverage (∼2.3 ML, Figure 4f), additional islands (υ) of considerable height (2.20 ± 0.02 nm, see Figure S8 with respect to the **LL** phase) are observed. This might be the onset of a Stranski−Krastanov growth,[59] leading to the formation of a TiO_2 3D-structure, which is probably the rutile $TiO_2(110)-(1 \times 1)$, as observed on W(100) at similar coverages.[9]

Theoretical DFT-Based Modeling. The unprecedented transition between the **QH** and **LL** structures occurring just above 1 ML coverage of the Cu(001) substrate, observed by LEED and STM, has been rationalized, thanks to DFT calculations.

https://doi.org/10.1021/acs.jpcc.1c01098
J. Phys. Chem. C 2021, 125, 10621−10630

The computed structural and electronic properties of the **LL**$p(3 \times 7)$ and **QH**$p(2 \times 7)$ structures are reported in Figure 5 and Table 1.

Table 1. Relevant Interface Properties Such as Distances between Planes, Adhesion and Strain Energies, Charge Transfer, and Fermi Energy Calculated for all the DFT-Investigated Structures[a]

	QH $p(2 \times 7)$	**LL** $p(3 \times 7)$
d_{12}[b]	1.090 (0.972)	1.165 (1.030)
d_{23}	0.939 (0.972)	0.548 (0.616)
d_{34}		0.986 (1.006)
d_{45}		0.630 (0.616)
d_{56}		1.044 (1.030)
d_{Cu-O}	2.031	1.917
E^{str}[c]	0.09 (0.01)	0.15 (0.02)
E_{adh}[d]	−23 (−0.18)	−9 (−0.05)
E^{str}_{adh}[e]	−22 (−0.17)	−7 (−0.03)
E^{str}_{adh} PBE0-D2*	−42 (−0.32)	−18 (−0.10)
E^{str}_{adh} B3LYP-D2*	−43 (−0.33)	−21 (−0.12)
CT ($\times 10^{-3}$)[f]	27	16
E_f (Δ)[g]	−5.63 (−1.02)	−5.55 (−0.94)

[a]Unless otherwise specified, all calculations are performed using the PW91 functional. In other cases, energy estimates have been carried out on the PW91 optimized geometry. When applicable, all calculations have been BSSE-corrected. [b]Distance in Å, see Figure 5 for labeling of the planes. Values for the unsupported film in brackets. [c]Defined as the difference between the energy of the fully relaxed film and the film relaxed at the substrate lattice parameters. All energies in meV/Å^2 (eV/TiO_2 in brackets). [d]Computed for an overlayer relaxed at the substrate lattice parameters. [e]Strained adhesion energy defined as $E^{str}_{adh} = E_{adh} + E^{str}$. [f]Charge transfer from the metal to TiO_2 expressed as charge per surface unit in |e|/Å^2. [g]Expressed in eV; in brackets, the difference Δ with respect to the bare metal is reported.

We address all the details of the DFT investigations of the Cu slab and unsupported films in the Supporting Information. For the supported films, the TiO_2 overlayers have been adsorbed on the metal surface with the bottom layer oxygen atoms located on top of the Cu atoms, being the favored registry for all metal-supported oxides.[17,20,60−64]

We first focus on the DFT investigation of the interface between the TiO_2-**QH** film and Cu(001) depicted, whose main properties are summarized in Table 1. Figure 5a reports the computed TiO_2-**QH**/Cu structure: a TiO_2 overlayer consists of a (2×6) oxide superstructure, a_0 = 5.20 Å and b_0 = 18.00 Å , and it is supported on the $p(2 \times 7)$ metal coincidence cell (blue), a = 5.12 and b = 17.87 Å , with a mismatch percentage of −1.54 and −0.72% for a_0 and b_0, respectively. The angle α between a_0 and b_0 is 118.6°, confirming a marginal deformation of the TiO_2-**QH**/Cu cell compared to the perfect hexagonal morphology of the unsupported film. This turns out in a value of the strain energy, E^{str} = 0.09 meV/Å^2 (0.01 eV/TiO_2), which is actually negligible. The **QH** adhesion energy, E_{adh}, at the interface, computed versus an unsupported film (which has been relaxed by keeping fixed the cell parameters at the values when it is supported), is −23 meV/Å^2 (−0.18 eV/TiO_2) and compensates for the strain energy. Indeed, the strain−adhesion energy balance indicates that the **QH** overlayer is thermodynamically more stable than the unsupported film, E^{str}_{adh} = −22 meV/Å^2 (−0.17 eV/TiO_2). The interface spacing (d_{Cu-O}) is 2.03 Å, roughly the sum of Cu and O covalent radii; d_{12} (the distance between the layer of the interface oxygens and the adjacent layer of titanium atoms) is 1.09 Å, significantly longer than in the unsupported film. All the other interlayer distances are very similar for the supported and unsupported oxide, see Table 1.

The bonding at the TiO_2-**QH**/Cu interface is characterized by direct Cu−O interaction with overlap between the O 2p state of oxygen atoms at the interface and the Cu 3d states (see c-PDOS in Figure S9). The bonding is accompanied by a charge transfer from the Cu 3d states of the surface in favor of the Ti 3d orbitals in the conduction band, CT = 27 × 10^{-3} |e|/Å^2, and by the downshift of the Fermi level (E_f = −5.63 eV) versus the Cu bare substrate (E_f = −4.61 eV), Table 1. The projected density of states, c-PDOS, is consistent with these findings: an examination of Figure S9 shows an upshift of the occupied O 2p and occupied Ti 3d bands together with a tiny downshift of the Ti virtual 3d states. Consequently, the band gap of the TiO_2 film is considerably reduced, and metal-induced gap states (predominantly Ti 3d derived states) appear close to the Fermi level. Such states, which are close to the conduction band of the oxide, show an acceptor-like character in agreement with the flow of charge from the metal to the oxide. The charge transfer also appears to be the driving mechanism for the considerable downshift of the Fermi level of the metal-oxide system compared to the bare substrate (see refs 65 and 66 for a more detailed discussion).

In a previous investigation of the **QH** structure on Cu(001), a smaller $c(2 \times 6)$ coincidence cell was instead used[20] as an approximation of the $p(2 \times 7)$ mesh derived by LEED experiments; despite a computed larger strain for the smaller $c(2 \times 6)$ overlayer, the properties of the oxide film described by the two models turn out to be fully comparable.

We now focus on the TiO_2-**LL** film on Cu(001), Figure 5b. Here, the TiO_2 overlayer consists of a (2×6) oxide superstructure, a_0 = 7.47 Å and b_0 = 18.18 Å , supported on a $p(3 \times 7)$ metal coincidence cell (blue), a = 7.66 and b = 17.87 Å . Also in this case, the interface is characterized by a small mismatch, +2.54 and −1.71% for a_0 and b_0, respectively, and a small strain energy, E^{str} = 0.15 meV/Å^2 (0.02 eV/TiO_2). The resulting interface energy, E^{str}_{adh} = −7 meV/Å^2 (−0.03 eV/TiO_2), considerably smaller than in the TiO_2-**QH**/Cu case, is indeed not due to the energy cost the oxide layer has to pay to match the periodicity of the metal substrate but rather due to the bond properties of the interface.

The main difference with respect to the TiO_2-**QH**/Cu interface is the smaller charge transfer from the metal to the oxide (CT = 16 × 10^{-3} |e|/Å^2) with a concomitantly less significant upshift of the work function: c-PDOS curves of Figure S9 show only a tiny accumulation of charge density just below the Fermi level due to the acceptor character of Ti 3d states.

TiO_2-**LL** overlayers have been observed on the Ag(100)[17] and Pt(111)[10] surfaces with adhesion energies E^{str}_{adh} of −23 and −14 meV/Å^2, respectively, to be compared with the value of −7 meV/Å^2 computed in this work. Despite the considerably larger interface energy, the TiO_2 film was found to be commensurate with the metal substrate only along one direction in the case of Ag(100) and not commensurate at all for Pt(111) because of the large strain energy required to match the metal periodicity. Therefore, the epitaxial growth of the TiO_2 film is likely driven by the morphology of the metal substrate and, more properly, by the lattice mismatch between the oxide layer and the substrate that is at the origin of the deformation of the oxide film. This could explain why the **QH**

https://doi.org/10.1021/acs.jpcc.1c01098
J. Phys. Chem. C 2021, 125, 10621−10630

phase (and the **QH** to **LL** transition) has not been observed on silver or platinum surfaces.[12,18]

It is worth noticing that previous studies have underlined that GGA methods usually tend to underestimate the binding energy of weakly interacting systems.[10,17,20] Noncovalent interactions have been accounted for by employing the B3LYP-D2* and PBE0-D2* schemes (see Computational Details in the Supporting Information). Interface energies computed within this approach are considerably increased, but the relative strength of the two interfaces is retained (see Table 1). This finding points out that the bonding at the interface, although based on a charge transfer mechanism, exhibits a significant contribution from noncovalent interactions due to the large polarizability of Cu and O atoms. Despite the stronger adhesion energy (E_{adh}^{str}) of the **QH** structure with respect to the **LL** one (Table 1), the **QH** phase turned out to be less thermodynamically stable than the **LL** phase, as measured by the computed formation energies E_f (calculated with respect to O and Ti atoms) that are −21.05 and −21.33 eV/TiO_2 for **QH** and **LL** films, respectively. This finding can explain the only presence of the TiO_2-**LL** structure observed by STM at high coverage (1.8 ML, Figure 4e).

Electronic Structure Evaluation by UPS. Finally, the electronic structure of the TiO_2 ultrathin films was studied by UPS and rationalized in light of the DOS simulations. Figure 6 reports the experimental UPS spectra of the TiO_2-**QH** film (0.8 ML) and the TiO_2-**LL** (1.8 ML) film on Cu(001) together with the total DOS (c-TDOS) of the **QH** and **LL** structure, respectively. The overall line-shape change in the UPS spectra that can be observed between 0.8 and 1.8 ML (i.e., **QH** and **LL** structures, respectively) is nicely reproduced by our computed DOS spectra (Figure 6). We observe that for both **QH** and **LL** structures, the UPS spectra at high energies (region ii) are dominated by the O 2p states, while the Cu 4s and Ti 3d subshell contribution is almost negligible. Close to the Fermi level (region i), the most relevant contribution is given by the Cu 3d subshell states coming from the substrate. Indeed, the UPS spectrum of the clean Cu(001) surface (see Figure S10) is characterized by Cu 3d bands located between −2 and −4 eV[67] from the Fermi level (region i). In the simulated spectra [computed in states*Mb/Hartree/cell vs $E-E_F$ (eV)], the Fermi level is shifted to be equal to that computed at the PWGGA level of calculation that corresponds to −5.63 and −5.55 eV for **QH** and **LL**, respectively. All the experimental UPS spectra were calibrated to the Cu(001) Fermi level. The shift between the UPS and the DOS spectra is intrinsic to the employed calculation methods.[68]

By comparing the UPS spectra of the **QH** and **LL** structures, a shift of the main feature (* in Figure 6) of 0.4 eV (from −4.6 to −5 eV) is observed, while c-PDOS O 2p contributions only differ by less than 0.1 eV. Therefore, the shift in the experimental data can be attributed to the presence of defects in real samples that are not taken into account in the calculations. Indeed, this could be due to an increase in the concentration of O vacancies passing from the **QH** to the **LL** structure.[69,70] This is also in agreement with the lower amount of Ti^{III} detected by XPS for the **QH** structure compared to the **LL** one.

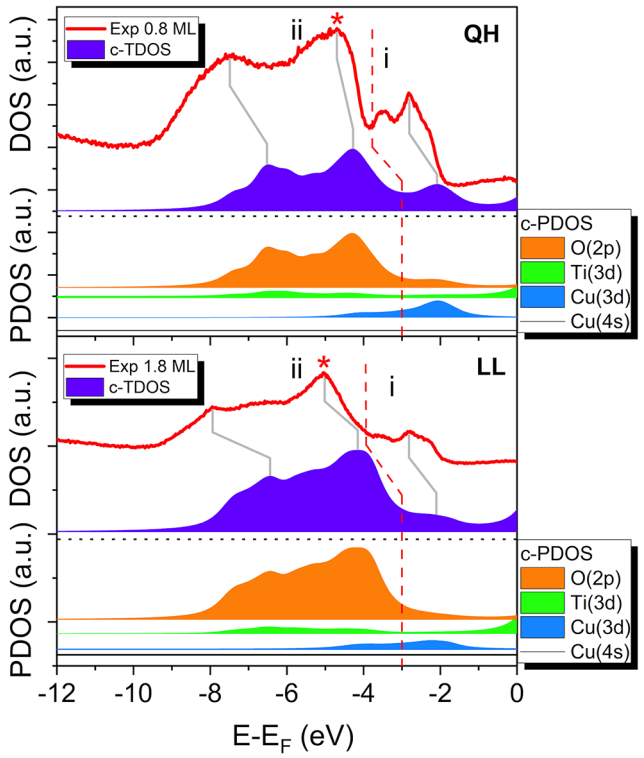

Figure 6. He(II) UPS spectra of the **QH** (top panel) and **LL** (bottom panel) structures. The c-PDOS (see the text) of the relevant photoionization subshells, weighted by subshell photoionization cross sections (in Mb), calculated for the **QH** and TiO_2-**LL** structure on Cu(001) are reported in each panel below the respective UPS spectrum.

CONCLUSIONS

We reported a detailed investigation of the TiO_2 ultrathin film growth on Cu(001). The growth has been carried out starting from the clean Cu(001) up to about 2 ML coverage. LEED, STM, and UPS results reveal that a structural change in the TiO_2 film occurs around 1.5 ML. In particular, it has been observed that the structure changes from a **QH** structure (present below 1 ML) to an **LL** structure, the latter is never observed so far on the Cu(001) surface. Our measurements suggest that a further structural change in the film to a 3D structure occurs above 2.0 ML. DFT calculations, performed to rationalize the structure of the TiO_2 film, indicate that the TiO_2-**QH** structure bound more strongly to the Cu substrate than the **LL** one, due to a significantly larger charge transfer from the metal to the Ti acceptors of the oxide occurring in the **QH** structure. Nevertheless, the TiO_2-**LL** structure turned out to be more thermodynamically stable, and thus, it replaces the **QH** one above 1 ML coverage. The understanding of the TiO_2 growth as the ultrathin film (i.e., in the mono- and bilayer regime) on Cu(001) achieved in this study is of major importance for the development of new TiO_2-based interfaces and devices. In light of a renewed interest in metal oxides as decoupling layers for atoms and molecules on metal surfaces,[25,26] we envision that the different bonding and charge transfer observed between the Cu substrate and the **QH** and **LL** TiO_2 phase could significantly influence the properties of the adsorbed species, leading to a deeper understanding of their interaction.[27]

ASSOCIATED CONTENT

Supporting Information

The Supporting Information is available free of charge at https://pubs.acs.org/doi/10.1021/acs.jpcc.1c01098.

https://doi.org/10.1021/acs.jpcc.1c01098
J. Phys. Chem. C 2021, 125, 10621−10630

Additional XPS, UPS spectra, LEED, STM images, DFT calculations, and **QH** to **LL** transition in TiO_2 ultrathin films on Cu(001) (PDF)

AUTHOR INFORMATION

Corresponding Authors

Giulia Serrano − *Department of Chemistry "U. Schiff"—DICUS—and INSTM Research Unit, University of Florence, 50019 Florence, Italy; Department of Industrial Engineering—DIEF—and INSTM Research Unit, University of Florence, 50139 Florence, Italy;* orcid.org/0000-0001-7953-7780; Email: giulia.serrano@unifi.it

Matteo Mannini − *Department of Chemistry "U. Schiff"—DICUS—and INSTM Research Unit, University of Florence, 50019 Florence, Italy;* orcid.org/0000-0001-7549-2124; Email: matteo.mannini@unifi.it

Authors

Andrea Luigi Sorrentino − *Department of Chemistry "U. Schiff"—DICUS—and INSTM Research Unit, University of Florence, 50019 Florence, Italy; Department of Industrial Engineering—DIEF—and INSTM Research Unit, University of Florence, 50139 Florence, Italy;* orcid.org/0000-0002-9476-4583

Lorenzo Poggini − *Department of Chemistry "U. Schiff"—DICUS—and INSTM Research Unit, University of Florence, 50019 Florence, Italy; Institute for Chemistry of Organo Metallic Compounds (ICCOM-CNR), 50019 Florence, Italy;* orcid.org/0000-0002-1931-5841

Brunetto Cortigiani − *Department of Chemistry "U. Schiff"—DICUS—and INSTM Research Unit, University of Florence, 50019 Florence, Italy*

Khaled E. El-Kelany − *Institute of Nanoscience and Nanotechnology, Kafrelshiekh University, 33516 Kafrelskiekh, Egypt; Dipartimento di Chimica, Università di Torino and NIS—Nanostructured Interfaces and Surfaces—Inter-departmental centre, 10125 Torino, Italy;* orcid.org/0000-0001-8216-8496

Maddalena D'Amore − *Dipartimento di Chimica, Università di Torino and NIS—Nanostructured Interfaces and Surfaces—Inter-departmental centre, 10125 Torino, Italy;* orcid.org/0000-0002-4248-8767

Anna Maria Ferrari − *Dipartimento di Chimica, Università di Torino and NIS—Nanostructured Interfaces and Surfaces—Inter-departmental centre, 10125 Torino, Italy;* orcid.org/0000-0003-1465-2774

Andrea Atrei − *Dipartimento di Biotecnologie, Chimica e Farmacia, University of Siena, 53100 Siena, Italy;* orcid.org/0000-0002-8860-3353

Andrea Caneschi − *Department of Industrial Engineering—DIEF—and INSTM Research Unit, University of Florence, 50139 Florence, Italy;* orcid.org/0000-0001-5535-3469

Roberta Sessoli − *Department of Chemistry "U. Schiff"—DICUS—and INSTM Research Unit, University of Florence, 50019 Florence, Italy; Institute for Chemistry of Organo Metallic Compounds (ICCOM-CNR), 50019 Florence, Italy;* orcid.org/0000-0003-3783-2700

Complete contact information is available at: https://pubs.acs.org/10.1021/acs.jpcc.1c01098

Author Contributions

A.L.S., G.S., L.P., and B.C. prepared and characterized the TiO_2 ultrathin film. K.E.E.-K., M.D., and A.M.F. performed the DFT studies. A.A., A.C., R.S., and M.M. supervised the activities of the project. All the authors contributed to the discussion and preparation of the manuscript.

Funding

MIUR-Italy ("Progetto Dipartimenti di Eccellenza 2018−2022, ref. 96C1700020008" allocated to the Department of Chemistry "Ugo Schiff") and Fondazione Ente Cassa di Risparmio di Firenze (project SPINE-2 2020.1634).

Notes

The authors declare no competing financial interest.

ACKNOWLEDGMENTS

We acknowledge MIUR-Italy ("Progetto Dipartimenti di Eccellenza 2018−2022, ref. 96C1700020008" allocated to the Department of Chemistry "Ugo Schiff") and Fondazione Ente Cassa di Risparmio di Firenze (projects Project SPINE-2 2020.1634) for the economic support. Access to the HPC resources of CINECA (Iscra project HP10CFUGEW) has been highly appreciated.

REFERENCES

(1) Linsebigler, A. L.; Lu, G.; Yates, J. T. Photocatalysis on TiO_2 Surfaces: Principles, Mechanisms, and Selected Results. *Chem. Rev.* **1995**, *95*, 735−758.

(2) Hussain, S.; Cao, C.; Usman, Z.; Chen, Z.; Nabi, G.; Khan, W. S.; Ali, Z.; Butt, F. K.; Mahmood, T. Fabrication and Photovoltaic Characteristics of Cu_2O/TiO_2 Thin Film Heterojunction Solar Cell. *Thin Solid Films* **2012**, *522*, 430−434.

(3) Chambers, S. A.; Thevuthasan, S.; Farrow, R. F. C.; Marks, R. F.; Thiele, J. U.; Folks, L.; Samant, M. G.; Kellock, A. J.; Ruzycki, N.; Ederer, D. L.; et al. Epitaxial Growth and Properties of Ferromagnetic Co-Doped TiO_2 Anatase. *Appl. Phys. Lett.* **2001**, *79*, 3467−3469.

(4) Schwarz, K. CrO_2 Predicted as a Half-Metallic Ferromagnet. *J. Phys. F: Met. Phys.* **1986**, *16*, L211−L215.

(5) Kadoshima, M.; Hiratani, M.; Shimamoto, Y.; Torii, K.; Miki, H.; Kimura, S.; Nabatame, T. Rutile-Type TiO_2 Thin Film for High-k Gate Insulator. *Thin Solid Films* **2003**, *424*, 224−228.

(6) Kim, S. K.; Kim, W.-D.; Kim, K.-M.; Hwang, C. S.; Jeong, J. High Dielectric Constant TiO_2 Thin Films on a Ru Electrode Grown at 250°C by Atomic-Layer Deposition. *Appl. Phys. Lett.* **2004**, *85*, 4112−4114.

(7) Rossella, F.; Galinetto, P.; Mozzati, M. C.; Malavasi, L.; Diaz Fernandez, Y.; Drera, G.; Sangaletti, L. TiO_2 Thin Films for Spintronics Application: A Raman Study. *J. Raman Spectrosc.* **2009**, *41*, 558−565.

(8) Khan, A. F.; Mehmood, M.; Durrani, S. K.; Ali, M. L.; Rahim, N. A. Structural and Optoelectronic Properties of Nanostructured TiO_2 Thin Films with Annealing. *Mater. Sci. Semicond. Process.* **2015**, *29*, 161−169.

(9) Harrison, G. T.; Spadaro, M. C.; Pang, C. L.; Grinter, D. C.; Yim, C. M.; Luches, P.; Thornton, G. Lepidocrocite-like TiO_2 and TiO_2 (110)−(1 × 2) Supported on W(100). *Mater. Sci. Technol.* **2016**, *32*, 203−208.

(10) Zhang, Y.; Giordano, L.; Pacchioni, G.; Vittadini, A.; Sedona, F.; Finetti, P.; Granozzi, G. The Structure of a Stoichiometric TiO_2 Nanophase on Pt(111). *Surf. Sci.* **2007**, *601*, 3488−3496.

(11) Matsumoto, T.; Batzill, M.; Hsieh, S.; Koel, B. E. Fundamental Studies of Titanium Oxide-Pt(100) Interfaces I. Stable High Temperature Structures Formed by Annealing TiO_x Films on Pt(100). *Surf. Sci.* **2004**, *572*, 127−145.

(12) Agnoli, S.; Orzali, T.; Sambi, M.; Vittadini, A.; Casarin, M.; Granozzi, G. Ultrathin TiO_2 Films on (1 × 2)-Pt(110): A LEED,

Photoemission, STM, and Theoretical Investigation. *J. Phys. Chem. C* **2008**, *112*, 20038−20049.
(13) Papageorgiou, A. C.; Cabailh, G.; Chen, Q.; Resta, A.; Lundgren, E.; Andersen, J. N.; Thornton, G. Growth and Reactivity of Titanium Oxide Ultrathin Films on Ni(110). *J. Phys. Chem. C* **2007**, *111*, 7704−7710.
(14) Atrei, A.; Bardi, U.; Rovida, G. Structure and Composition of the Titanium Oxide Layers Formed by Low-Pressure Oxidation of the $Ni_{94}Ti_6$(110) Surface. *Surf. Sci.* **1997**, *391*, 216−225.
(15) Diebold, U. The Surface Science of Titanium Dioxide. *Surf. Sci. Rep.* **2003**, *48*, 53−229.
(16) Reyes-Coronado, D.; Rodríguez-Gattorno, G.; Espinosa-Pesqueira, M. E.; Cab, C.; De Coss, R.; Oskam, G. Phase-Pure TiO_2 Nanoparticles: Anatase, Brookite and Rutile. *Nanotechnology* **2008**, *19*, 145605.
(17) Atrei, A.; Ferrari, A. M.; Szieberth, D.; Cortigiani, B.; Rovida, G. Lepidocrocite-like Structure of the TiO_2 Monolayer Grown on Ag(100). *Phys. Chem. Chem. Phys.* **2010**, *12*, 11587−11595.
(18) Kaneko, H.; Ono, M.; Ozawa, K.; Edamoto, K. Growth of Ordered Titanium Oxide Films on Ag(100). *Solid State Commun.* **2007**, *142*, 32−35.
(19) Finetti, P.; Caffio, M.; Cortigiani, B.; Atrei, A.; Rovida, G. Mechanism of Growth and Structure of Titanium Oxide Ultrathin Films Deposited on Cu(001). *Surf. Sci.* **2008**, *602*, 1101−1113.
(20) Atrei, A.; Ferrari, A. M.; Finetti, P.; Beni, A.; Rovida, G. LEED and DFT Study of the Quasihexagonal TiO_2 Structure on Cu(001). *J. Phys. Chem. C* **2009**, *113*, 19578−19584.
(21) Seo, H. O.; Park, S.-Y.; Shim, W. H.; Kim, K.-D.; Lee, K. H.; Jo, M. Y.; Kim, J. H.; Lee, E.; Kim, D.-W.; Kim, Y. D.; et al. Ultrathin TiO_2 Films on Zno Electron-Collecting Layers of Inverted Organic Solar Cell. *J. Phys. Chem. C* **2011**, *115*, 21517−21520.
(22) Tosoni, S.; Pacchioni, G. Hydrogen Adsorption on Free-Standing and Ag-Pt Supported TiO_2 Thin Films. *J. Phys. Chem. C* **2019**, *123*, 7952−7960.
(23) Wang, S. L.; Luo, X.; Zhou, X.; Zhu, Y.; Chi, X.; Chen, W.; Wu, K.; Liu, Z.; Quek, S. Y.; Xu, G. Q. Fabrication and Properties of a Free-Standing Two-Dimensional Titania. *J. Am. Chem. Soc.* **2017**, *139*, 15414−15419.
(24) Reeves, K. G.; Ma, J.; Fukunishi, M.; Salanne, M.; Komaba, S.; Dambournet, D. Insights into Li+, Na+, and K+ Intercalation in Lepidocrocite-Type Layered TiO_2 Structures. *ACS Appl. Energy Mater.* **2018**, *1*, 2078−2086.
(25) Baumann, S.; Paul, W.; Choi, T.; Lutz, C. P.; Ardavan, A.; Heinrich, A. J. Electron Paramagnetic Resonance of Individual Atoms on a Surface. *Science* **2015**, *350*, 417−420.
(26) Wäckerlin, C.; Donati, F.; Singha, A.; Baltic, R.; Rusponi, S.; Diller, K.; Patthey, F.; Pivetta, M.; Lan, Y.; Klyatskaya, S.; et al. Giant Hysteresis of Single-Molecule Magnets Adsorbed on a Nonmagnetic Insulator. *Adv. Mater.* **2016**, *28*, 5195−5199.
(27) Tosoni, S.; Pacchioni, G. Bonding Properties of Isolated Metal Atoms on Two-Dimensional Oxides. *J. Phys. Chem. C* **2020**, *124*, 20960−20973.
(28) Serrano, G.; Velez-Fort, E.; Cimatti, I.; Cortigiani, B.; Malavolti, L.; Betto, D.; Ouerghi, A.; Brookes, N. B.; Mannini, M.; Sessoli, R. Magnetic Bistability of $TbPc_2$ Submonolayer on a Graphene/SiC(0001) Conductive Electrode. *Nanoscale* **2018**, *10*, 2715−2720.
(29) Finetti, P.; Sedona, F.; Rizzi, G. A.; Mick, U.; Sutara, F.; Svec, M.; Matolin, V.; Schierbaum, K.; Granozzi, G. Core and Valence Band Photoemission Spectroscopy of Well-Ordered Ultrathin TiO_x Films on Pt(111). *J. Phys. Chem. C* **2007**, *111*, 869−876.
(30) Alexander, M. R.; Thompson, G. E.; Zhou, X.; Beamson, G.; Fairley, N. Quantification of Oxide Film Thickness at the Surface of Aluminium Using XPS. *Surf. Interface Anal.* **2002**, *34*, 485−489.
(31) Végh, J. The Analytical Form of the Shirley-Type Background. *J. Electron Spectrosc. Relat. Phenom.* **1988**, *46*, 411−417.
(32) Dovesi, R.; Saunders, V. R.; Roetti, C.; Orlando, R.; Zicovich-Wilson, C. M.; Pascale, F.; Civalleri, B.; Doll, K.; Harrison, N. M.; Bush, I. J.; D'Arco, P.; Llunell, M.; Causà, M.; Noël, Y.; Maschio, L.; Erba, A.; Rerat, M. *S. C. CRYSTAL17. CRYSTAL17 User's Man*; University of Turin: Torino, 2017.
(33) Grimme, S.; Antony, J.; Ehrlich, S.; Krieg, H. A Consistent and Accurate Ab Initio Parametrization of Density Functional Dispersion Correction (DFT-D) for the 94 Elements H-Pu. *J. Chem. Phys.* **2010**, *132*, 154104.
(34) Fornaro, T.; Brucato, J. R.; Feuillie, C.; Sverjensky, D. A.; Hazen, R. M.; Brunetto, R.; D'Amore, M.; Barone, V. Binding of Nucleic Acid Components to the Serpentinite-Hosted Hydrothermal Mineral Brucite. *Astrobiology* **2018**, *18*, 989−1007.
(35) Signorile, M.; Vitillo, J. G.; D'Amore, M.; Crocella, V.; Ricchiardi, G.; Bordiga, S. Characterization and Modelling of Reversible CO2 Capture From Wet Streams by a MgO/zeolite Y Nanocomposite. *J. Phys. Chem. C* **2019**, *123* (28), 17214−17224.
(36) Korotcenkov, G.; Brinzari, V.; Hanyš, P.; Nehasil, V. XPS Study of the SnO_2 Films Modified with Rh. *Surf. Interface Anal.* **2018**, *50*, 795−801.
(37) Diebold, U.; Madey, T. E. TiO_2 by XPS. *Surf. Sci. Spectra* **1996**, *4*, 227−231.
(38) Oh, W. S.; Xu, C.; Kim, D. Y.; Goodman, D. W. Preparation and Characterization of Epitaxial Titanium Oxide Films on Mo(100). *J. Vac. Sci. Technol., A* **1997**, *15*, 1710−1716.
(39) Mayer, J. T.; Diebold, U.; Madey, T. E.; Garfunkel, E. Titanium and Reduced Titania Overlayers on Titanium Dioxide(110). *J. Electron Spectrosc. Relat. Phenom.* **1995**, *73*, 1−11.
(40) Jackman, M. J.; Thomas, A. G.; Muryn, C. Photoelectron Spectroscopy Study of Stoichiometric and Reduced Anatase TiO_2(101) Surfaces: The Effect of Subsurface Defects on Water Adsorption at near-Ambient Pressures. *J. Phys. Chem. C* **2015**, *119*, 13682−13690.
(41) Oku, M.; Wagatsuma, K.; Kohiki, S. Ti 2p and Ti 3p X-Ray Photoelectron Spectra for TiO_2, $SrTiO_3$ and $BaTiO_3$. *Phys. Chem. Chem. Phys.* **1999**, *1*, 5327−5331.
(42) Kim, K. S.; Winograd, N. Charge Transfer Shake-up Satellites in X-Ray Photoelectron Spectra of Cations and Anions of $SrTiO_3$, TiO_2 and Sc_2O_3. *Chem. Phys. Lett.* **1975**, *31*, 312−317.
(43) Fan, C.; Chen, C.; Wang, J.; Fu, X.; Ren, Z.; Qian, G.; Wang, Z. Black Hydroxylated Titanium Dioxide Prepared via Ultrasonication with Enhanced Photocatalytic Activity. *Sci. Rep.* **2015**, *5*, 11712.
(44) Zhou, B.; Jiang, X.; Liu, Z.; Shen, R.; Rogachev, A. V. Preparation and Characterization of TiO_2 Thin Film by Thermal Oxidation of Sputtered Ti Film. *Mater. Sci. Semicond. Process.* **2013**, *16*, 513−519.
(45) Serrano, G.; Bonanni, B.; Di Giovannantonio, M.; Kosmala, T.; Schmid, M.; Diebold, U.; Di Carlo, A.; Cheng, J.; VandeVondele, J.; Wandelt, K.; et al. Molecular Ordering at the Interface Between Liquid Water and Rutile TiO_2 (110). *Adv. Mater. Interfaces* **2015**, *2*, 1500246.
(46) Malavolti, L.; Poggini, L.; Margheriti, L.; Chiappe, D.; Graziosi, P.; Cortigiani, B.; Lanzilotto, V.; de Mongeot, F. B.; Ohresser, P.; Otero, E.; et al. Magnetism of $TbPc_2$ SMMs on Ferromagnetic Electrodes Used in Organic Spintronics. *Chem. Commun.* **2013**, *49*, 11506−11508.
(47) Zhang, L.; Persaud, R.; Madey, T. E. Ultrathin Metal Films on a Metal Oxide Surface: Growth of Au on (110). *Phys. Rev. B: Condens. Matter Mater. Phys.* **1997**, *56*, 10549−10557.
(48) Simmons, G. W.; Mitchell, D. F.; Lawless, K. R. Leed and Heed Studies of the Interaction of Oxygen with Single Crystal Surfaces of Copper. *Surf. Sci.* **1967**, *8*, 130−164.
(49) McDonnell, L.; Woodruff, D. P.; Mitchell, K. A. R. Constant Momentum Transfer Averaging in LEED; Analysis of a Structure of Oxygen on Cu (100). *Surf. Sci.* **1974**, *45*, 1−19.
(50) Braithwaite, M. J.; Joyner, R. W.; Roberts, M. W. Interaction of Oxygen with Cu (100) Studied by Low Energy Electron Diffraction (LEED) and X-Ray Photoelectron Spectroscopy (XPS). *Faraday Discuss. Chem. Soc.* **1975**, *60*, 89−101.
(51) Atrei, A.; Bardi, U.; Rovida, G.; Zanazzi, E.; Casalone, G. Test of Structural Models for Cu(001)-($\sqrt{2} \times 2\sqrt{2}$) R45°-O by LEED Intensity Analysis. *Vacuum* **1990**, *41*, 333−336.

https://doi.org/10.1021/acs.jpcc.1c01098
J. Phys. Chem. C 2021, 125, 10621−10630

(52) Suggs, D. W.; Bard, A. J. Scanning Tunneling Microscopic Study with Atomic Resolution of the Dissolution of Cu(100) Electrodes in Aqueous Chloride Media. *J. Phys. Chem.* **1995**, *99*, 8349−8355.
(53) Højrup Hansen, K.; Worren, T.; Lægsgaard, E.; Besenbacher, F.; Stensgaard, I. Bias Dependent Apparent Height of an Al_2O_3 Thin Film on NiAl(110), and of Supported Pd Clusters. *Surf. Sci.* **2001**, *475*, 96−102.
(54) Sebastian, I.; Neddermeyer, H. Scanning Tunneling Microscopy on the Atomic and Electronic Structure of CoO Thin Films on Ag(100). *Surf. Sci.* **2000**, *454*−*456*, 771−777.
(55) Wu, C.; Marshall, M. S. J.; Castell, M. R. Surface Structures of Ultrathin TiO_x Films on Au (111). *J. Phys. Chem. C* **2011**, *115*, 8643−8652.
(56) Liu, B.-H.; Boscoboinik, J. A.; Cui, Y.; Shaikhutdinov, S.; Freund, H.-J. Stabilization of Ultrathin Zinc Oxide Films on Metals: Reconstruction versus Hydroxylation. *J. Phys. Chem. C* **2015**, *119*, 7842−7847.
(57) Wen, H. F.; Miyazaki, M.; Zhang, Q.; Adachi, Y.; Li, Y. J.; Sugawara, Y. Direct Observation of Atomic Step Edges on the Rutile TiO_2 (110)-(1x1) Surface Using Atomic Force Microscopy. *Phys. Chem. Chem. Phys.* **2018**, *20*, 28331−28337.
(58) Atrei, A.; Cortigiani, B.; Ferrari, A. M. Epitaxial Growth of TiO_2 Films with the Rutile (110) Structure on Ag(100). *J. Phys.: Condens. Matter* **2012**, *24*, 445005.
(59) Männig, A.; Zhao, Z.; Rosenthal, D.; Christmann, K.; Hoster, H.; Rauscher, H.; Behm, R. J. Structure and Growth of Ultrathin Titanium Oxide Films on Ru(0001). *Surf. Sci.* **2005**, *576*, 29−44.
(60) Ferrari, A. M.; Pisani, C. An Ab Initio Periodic Study of NiO Supported at the Pd(100) Surface. Part 1: The Perfect Epitaxial Monolayer. *J. Phys. Chem. B* **2006**, *110*, 7909−7917.
(61) Ferrari, A. M.; Ferrero, M.; Pisani, C. An Ab Initio Periodic Study of NiO Supported at the Pd(100) Surface. Part 2: The Nonstoichiometric Ni_3O_4 Phase. *J. Phys. Chem. B* **2006**, *110*, 7918−7927.
(62) Arble, C.; Tong, X.; Giordano, L.; Ferrari, A. M.; Newberg, J. T. Water Dissociation on MnO(1×1)/Ag(100). *Phys. Chem. Chem. Phys.* **2016**, *18*, 25355−25363.
(63) Giordano, L.; Ferrari, A. M. Modified Ion Pair Interaction for Water Dimers on Supported MgO Ultrathin Films. *J. Phys. Chem. C* **2012**, *116*, 20349−20355.
(64) Arble, C.; Tong, X.; Giordano, L.; Newberg, J. T.; Ferrari, A. M. Terrace Site Hydroxylation upon Water Dimer Formation on Monolayer NiO/Ag(100). *Thin Solid Films* **2018**, *660*, 365−372.
(65) Sementa, L.; Barcaro, G.; Negreiros, F. R.; Thomas, I. O.; Netzer, F. P.; Ferrari, A. M.; Fortunelli, A. Work Function of Oxide Ultrathin Films on the Ag(100) Surface. *J. Chem. Theory Comput.* **2012**, *8*, 629−638.
(66) Cinquini, F.; Giordano, L.; Pacchioni, G.; Ferrari, A. M.; Pisani, C.; Roetti, C. Electronic Structure of NiO Ag(100) Thin Films from DFT+U and Hybrid Functional DFT Approaches. *Phys. Rev. B: Condens. Matter Mater. Phys.* **2006**, *74*, 165403.
(67) Lozzi, L.; Passacantando, M.; Picozzi, P.; Santucci, S.; den Daas, H. Oxidation of the Fe Cu(100) Interface. *Surf. Sci.* **1995**, *331*−*333*, 703−709.
(68) Cimatti, I.; Bondì, L.; Serrano, G.; Malavolti, L.; Cortigiani, B.; Velez-Fort, E.; Betto, D.; Ouerghi, A.; Brookes, N. B.; Loth, S.; et al. Vanadyl Phthalocyanines on Graphene/SiC(0001): Toward a Hybrid Architecture for Molecular Spin Qubits. *Nanoscale Horiz.* **2019**, *4*, 1202−1210.
(69) Tait, R. H.; Kasowski, R. V. Ultraviolet Photoemission and Low-Energy-Electron Diffraction Studies of TiO_2 (Rutile) (001) and (110) Surfaces. *Phys. Rev. B: Condens. Matter Mater. Phys.* **1979**, *20*, 5178−5191.
(70) Henrich, V. E.; Dresselhaus, G.; Zeiger, H. J. Observation of Two-Dimensional Phases Associated with Defect States on the Surface of TiO_2. *Phys. Rev. Lett.* **1976**, *36*, 1335−1339.

https://doi.org/10.1021/acs.jpcc.1c01098
J. Phys. Chem. C 2021, 125, 10621−10630